Control Engineering Practice 18 (2010) 700–711

Contents lists available at ScienceDirect

Control Engineering Practice

journal homepage: www.elsevier.com/locate/conengprac

Modeling, system identification and robust control of a coaxial micro helicopter

D. Schafroth *, C. Bermes, S. Bouabdallah, R. Siegwart

Autonomous Systems Lab, Tannenstr. 3, ETH Zurich, 8092 Zurich, Switzerland

ARTICLE INFO

Article history:
Received 2 April 2009
Accepted 2 February 2010
Available online 16 February 2010

Keywords:
Helicopter
Control
H-infinity
Identification
Model
Mixed sensitivity problem

ABSTRACT

In this paper the design process of robust H_∞- control for a coaxial micro helicopter is presented. The process starts with the development of a nonlinear dynamic model reflecting all the important elements of the helicopter. The corresponding system parameters are identified using measurement data from test benches and real flight, as well as a nonlinear identification tool, the Covariance Matrix Adaptation Evolution Strategy (CMA-ES). The identified and verified model is then used for the design of H_∞- controllers for attitude and heave control, which are successfully tested in flight on the real system.

1. Introduction

The interest in autonomous micro air vehicles (MAV) for tasks such as surveillance and security, search and rescue or inspection and exploration is still growing, and many vehicles are developed. Especially micro helicopters are in the focus of the researchers due to their ability to hover and their power to carry payload. Existing micro helicopters are for example the muFR helicopter developed by Epson (2004), the CoaX 2 developed at ETHZ (Bermes, Leutenegger, Bouabdallah, Schafroth, & Siegwart, 2008) and the MICOR developed by the University of Maryland (Bohorquez, Rankinsy, Baederz, & Pines, 2003). The goal of the European Framework project muFly is to develop a fully autonomous micro helicopter in the size and mass of a small bird. A big challenge and key point in the design of an autonomous helicopter in such a size is the feedback control. While the control of a full size and normal size RC-helicopter is already very difficult, the micro helicopter additionally suffers from faster dynamics, inaccurate actuators and low output quality of lightweight sensors. Nevertheless, a very tight feedback control is necessary for the foreseen missions and it is questionable if traditional control approaches like PID controllers are the right choice. It is more likely that higher order, model based controllers are a better choice and more effective. There exist many works, mainly on full scale helicopters, with various control techniques such as linear quadratic Gaussian control (Zhao & Murthy, 2009), fuzzy logic adaptive control (Wade & Walker, 1996), backstepping and sliding mode control (Bouabdallah & Siegwart, 2005), adaptive neural networks (Leitner, Calise, & Prasad, 1997) and many other methodologies. A strong interest exists in the H_∞-loop shaping method due to its robustness and structured design method. In Walker (2003) a comprehensive overview on the works on H_∞- controllers in the field of helicopters during the last 20 years is given, showing the complexity but also the strength of the design method. A work on the control of a coaxial micro helicopter is (Wang, Song, Nonami, Hirata, & Miyazawa, 2006) where PID control is combined with H_∞- control techniques. The goal of this work is to use different multiple input multiple output (MIMO) H_∞- controllers for an accurate control of the helicopter.

In order to have an appropriate model for the control and simulations, a nonlinear dynamic model for muFly is developed, including all the specialties like the stabilizer bar or the brushless DC motors. This model is based on the rigid body equation including all the attacking forces and moments around hover state. An important part of the control design and often not shown in literature is the verification of the used model and the parameter identification. In addition to the parameter identification on the ground and on test benches, identification on real flight data is needed. Only a few examples of the application of system identification techniques to model-scale helicopters exist and the results are, compared to full-scale helicopters, limited (Mettler, Kanade, & Tischler, 2000). Additionally, the models are mainly identified on the linearized state space system around hover. In general this gives good results but linear models are not able to cover all the existing effects. For example linearization

* Corresponding author. Tel.: +41 446328949; fax: +41 446321181.
E-mail address: sdario@ethz.ch (D. Schafroth).

0967-0661/$ - see front matter © 2010 Elsevier Ltd. All rights reserved.
doi:10.1016/j.conengprac.2010.02.004

cancels cross couplings between the angular rates. Moreover it is desirable to have an identified nonlinear model for accurate simulations and controller evaluation, even though the controller itself is linear. Another advantage of the nonlinear identification is that operation points for hover do not have to be estimated. In this work a nonlinear parameter identification based on the Covariance Matrix Adaptation Evolution Strategy (CMA-ES) (Hansen & Ostermeier, 1996) is presented. This randomized search algorithm allows for an accurate identification of systems with high dimensions and multiple parameters.

The paper is organized as follows. In Section 2 the muFly micro helicopter and its hardware setup is shown, followed by the nonlinear model in Section 3. The identification process with the CMA-ES is presented in Section 4. Section 5 presents the control design for muFly.

2. The muFly helicopter

muFly is a 17 cm in span, 15 cm in height coaxial helicopter (Fig. 1) with a mass of 95 g. The two rotors are driven by two lightweight brushless DC (BLDC) motors and are counter rotating to compensate the resulting torque due to aerodynamical drag. This allows to control the yaw by differential speed variation of the two rotors, whereas the altitude can be controlled varying the rotor speeds simultaneously. The motor speed is reduced by a gear in order to achieve a higher torque on the rotor side.

A benefit of the coaxial setup is that one rotor can be used to help stabilizing the helicopter using a stabilizer bar. Such devices, mounted on the upper rotor, are often found on RC-Models. The helicopter is steered by a conventional swash plate on the lower rotor actuated by two servos and powered by a lithium polymer battery. All the signals to the servos and motor controllers are pulse position modulated (PPM) signals.

Sensors mounted on the platform are an inertial measurement unit (IMU) and an ultrasonic distance sensor for the measurement of the distance to the ground. With this setup, the attitude angles and the height over ground can be measured. Further, an omnidirectional camera in combination with lasers is in development, that will be used together with a down-looking camera for position measurement. The sensor data is processed by a dsPIC microprocessor and sent to the ground station by a serial connection using a bluetooth module. In order to minimize time delays for the identification, the actuator inputs are sent in the same package as the sensor data. The same microprocessor is used for the control.

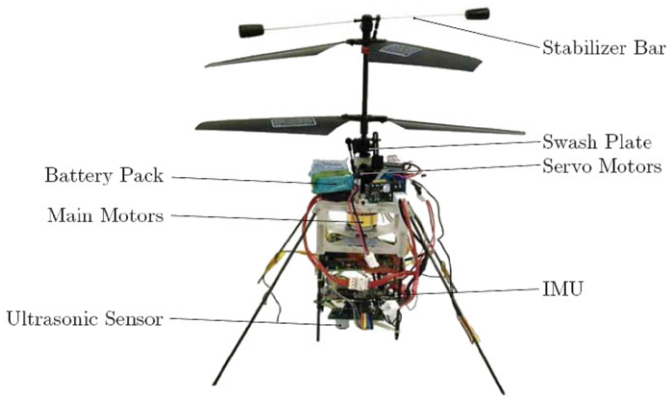

Fig. 1. The second prototype of the muFly helicopter.

3. Nonlinear model

The nonlinear model developed for the muFly project is a physical model based on the rigid body motion being presented in detail in Schafroth, Bermes, Bouabdallah, and Siegwart (2009). In this work, an overview is given, pointing out the specialties of the muFly helicopter. The goal of the model is to be as simple as possible, since it has to be used for the controller design. On the other hand, the physics and dynamics of the different components mounted on the muFly helicopter have to be reflected accurately.

As common in aeronautics, an inertial J frame and a body fixed frame B are introduced, resulting in the transformation equation for the position, velocities, angles and angular rates. Using Newtonian mechanics the differential equations for the rigid body motion in the body-fixed frame located at the helicopter's center of gravity (CoG) are

$$\begin{bmatrix}\dot{u}\\ \dot{v}\\ \dot{w}\end{bmatrix} = \frac{1}{m}\mathbf{f} - \begin{bmatrix}p\\ q\\ r\end{bmatrix} \times \begin{bmatrix}u\\ v\\ w\end{bmatrix}$$

and

$$\begin{bmatrix}\dot{p}\\ \dot{q}\\ \dot{r}\end{bmatrix} = \mathbf{I}^{-1}\left(\mathbf{m} - \begin{bmatrix}p\\ q\\ r\end{bmatrix} \times \mathbf{I}\begin{bmatrix}p\\ q\\ r\end{bmatrix}\right),$$

with the body velocities u, v, w, the system mass m, the angular velocities p, q, r the body inertia tensor $\mathbf{I}$ and the total external force and moment vectors $\mathbf{f}$ and $\mathbf{m}$. So far, the equations of motion are independent of the flying platform and can be found in literature, e.g. (Mettler, 2003). Now the platform dependent total external force $\mathbf{f}$ and moment $\mathbf{m}$ vectors have to be defined.

The forces and moments acting on muFly can be summarized as

$$\mathbf{f} = \mathbf{t}_{\text{up}} + \mathbf{t}_{\text{dw}} + \mathbf{g} + \mathbf{w}_{\text{hub}},$$

$$\mathbf{m} = \mathbf{q}_{\text{up}} + \mathbf{q}_{\text{dw}} + \mathbf{r}_{\text{Cup}} \times \mathbf{t}_{\text{up}} + \mathbf{r}_{\text{Cdw}} \times \mathbf{t}_{\text{dw}} + \mathbf{q}_{gyro,dw} + \mathbf{q}_{gyro,up},$$

with the terms: upper and lower rotor thrust vector $\mathbf{t}_{\text{up}}$ and $\mathbf{t}_{\text{dw}}$, gravity vector $\mathbf{g}$, aerodynamic fuselage drag $\mathbf{w}_{\text{hub}}$ and rotor drag torques $\mathbf{q}_{\text{up}}$ and $\mathbf{q}_{\text{dw}}$, gyroscopic torques of the rotors $\mathbf{q}_{\text{gyro,dw}}$, $\mathbf{q}_{\text{gyro,up}}$ and the moments due to the cross product of the forces not aligned with the CoG. Aerodynamic forces and moments on the fuselage due to translation in the air are neglected since the helicopter will mainly operate around hover condition. The next step is to define the single forces and moments.

The rotor thrust vector is defined as $\mathbf{t}_i$ and rotor torque vector $\mathbf{q}_i$ as $\mathbf{t}_i = T_i \cdot \mathbf{n}_{Ti}$ and $\mathbf{q}_i = Q_i \cdot \mathbf{n}_{Qi}$, with $i \in \{\text{dw}, \text{up}\}$ for the lower and upper rotor. In hover, the thrust and torque magnitude T_i and Q_i of a rotor with radius R can be defined as (Bramwell, 2001)

$$T_i = c_{Ti}\pi\rho R^4\Omega_i^2 = c_{Ti}k_T\Omega_i^2,$$

$$Q_i = c_{Qi}\pi\rho R^5\Omega_i^2 = c_{Qi}k_Q\Omega_i^2,$$

with air density ρ, the thrust and torque coefficient c_T and c_Q, and the rotor speed Ω_i.

The thrust vectors can be described using two tilt angles α_i and β_i around the x- and y-axis Fig. 2 as

$$\mathbf{n}_{Ti} = \begin{bmatrix}\cos\alpha_i \sin\beta_i\\ \sin\alpha_i\\ -\cos\alpha_i\cos\beta_i\end{bmatrix}.$$

The rotor torque vectors are assumed to act only in the rotor axis (z-axis), but it has to be considered that the lower rotor turns clockwise, while the upper rotor turns counterclockwise as seen from above.

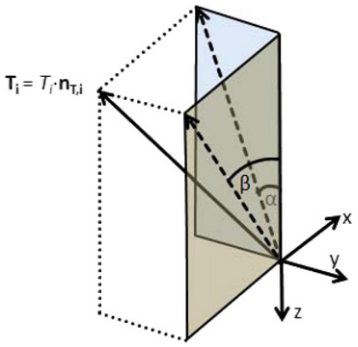

Fig. 2. Visualization of the tilted thrust vector with tilt angles α and β.

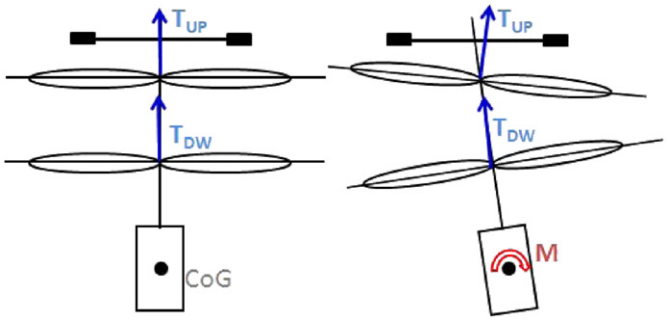

Fig. 3. The principle of the stabilizer bar. Due to the high inertia the stabilizer bar lags behind the roll/pitch movement, applies a cyclic pitch input to the rotor and creates a redress moment.

The last torques result from the acceleration of the rotors. For the case of the lower rotor this might be negligible, but the high inertia of the stabilizer bar, mounted on the upper rotor, causes a notable torque while accelerating the rotor. The gyroscopic torque vectors are assumed to act only in the rotor axis direction with the magnitude

$$Q_{gyro,i} = J_{drive,i}\dot{\Omega}_i.$$

Now the only missing part in the model is the dynamics of the stabilizer bar, swash plate, servos and electro motors.

An important part of the system model is the stabilizer bar. In simple words this stabilization mechanism gives cyclic pitch inputs, similar to the swash plate, to the upper rotor to stabilize the helicopter in flight. The stabilizer bar has a high inertia and lags behind a roll or pitch movement of the fuselage as shown in Fig. 3. Through a rigid connection to the rotor, this time delay results in a cyclic pitching of the rotor blades and therefore to a tilting of the tip path plane (TPP) (Leishman, 2006). If the stabilizer bar is adjusted correctly, the thrust vector points in the opposite direction of the roll or pitch movement causing a redress moment.

The stabilizer bar following the roll/pitch movement can be modeled as a first order element (Mettler, 2003) as

$$\dot{\eta}_{\text{bar}} = \frac{1}{T_{\text{f,up}}}(\phi - \eta_{\text{bar}}),$$

$$\dot{\zeta}_{\text{bar}} = \frac{1}{T_{\text{f,up}}}(\theta - \zeta_{\text{bar}}),$$

with the angles between the rotor axis and the normal of the stabilizer bar plane η_{bar} and ζ_{bar}, and the time constants $T_{f,up}$. The tilt angles of the thrust vector in the body-fixed frame are the differences between the two angles η_{bar} and ζ_{bar} and the roll and pitch angles scaled by a factor l_{up}, since the interest is in the tilt angle of the TPP and not that of the stabilizer bar. Thus the equations for the tilting angles for the thrust vector are

$$\alpha_{\text{up}} = l_{\text{up}}(\phi - \eta_{\text{bar}}),$$

$$\beta_{\text{up}} = l_{\text{up}}(\theta - \zeta_{\text{bar}}).$$

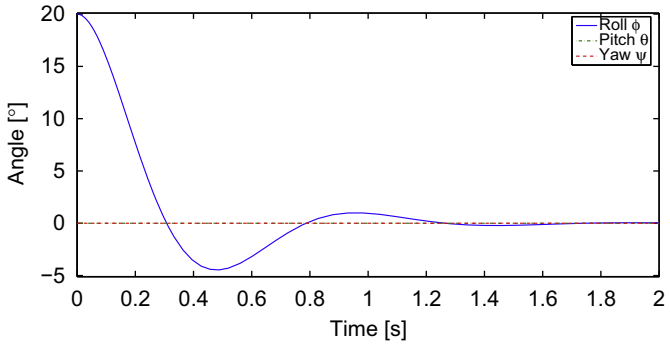

Fig. 4. The reaction of the helicopter to an initial roll displacement of 20° with the modeled stabilizer bar.

The influence of the modeled stabilizer bar is shown in Fig. 4, where the reaction of the helicopter to an initial displacement in the roll angle is plotted. After a short time period, the helicopter is back in the hover position.

The idea of the swash plate model is the same as for the stabilizer bar. The reaction from the servo input (PPM signal) to the change in the TPP is also modeled by a first order system. Hereby all the dynamics of the servos and rotor are covered by the time constant $T_{\text{f,dw}}$. The tilting angles of the lower rotor are modeled as

$$\dot{\alpha}_{\text{dw}} = \frac{1}{T_{\text{f,dw}}}(-l_{\text{dw}}u_{\text{serv2}} \cdot \theta_{\text{SPmax}} - \alpha_{\text{dw}}),$$

$$\dot{\beta}_{\text{dw}} = \frac{1}{T_{\text{f,dw}}}(-l_{\text{dw}}u_{\text{serv1}} \cdot \theta_{\text{SPmax}} - \beta_{\text{dw}}),$$

with the time constant $T_{\text{f,dw}}$, scaling factor l_{dw}, maximal swash plate tilting angle θ_{SPmax} and servo inputs $u_{\text{serv},i}$.

Since the motor-controllers for the BLDC motors do not have a speed control and no speed measurement output, the electro motors have to be modeled as well. The equations for the rotor speeds Ω_i are based on the well known electro motor equation (Mueller & Ponick, 2006) and extended by the gear resulting in the final equation

$$J_{\text{drive}}\dot{\Omega}_i = \frac{\kappa_{\text{M}}U_{\text{bat}}u_{\text{mot},i} - \kappa_{\text{M}}\kappa_{\text{E}}i_{\text{gear}}\Omega_i}{i_{\text{gear}}R_{\Omega}} - d_R\Omega_i - \frac{c_{Qi}k_Q\Omega_i^2}{i_{\text{gear}}^2 \cdot \eta_{\text{gear}}},$$

with the moment of inertia J_{mot}, the electrical and mechanical motor constants κ_{E} and κ_{M}, the electrical resistance R_{Ω}, the friction coefficient d_R the gear ratio i_{gear}, the efficiency of the gear η_{gear}, the battery voltage U_{bat} and the motor input $u_{\text{mot},i}$.

All the equations result in a nonlinear model with 18 states

$$\mathbf{x} = [x, y, z, u, v, w, \phi, \theta, \psi, p, q, r, \alpha_{\text{dw}}, \beta_{\text{dw}}, \alpha_{\text{up}}, \beta_{\text{up}}, \Omega_{\text{dw}}, \Omega_{\text{up}}]^T$$

and four inputs (the two motors and the two servos)

$$\mathbf{u} = [u_{\text{mot,dw}}, u_{\text{mot,up}}, u_{\text{serv1}}, u_{\text{serv2}}]^T$$

scaled to $u_{\text{serv}} \in \{-1, 1\}$ and $u_{\text{mot}} \in \{0, 1\}$. The nonlinear model is shown in Fig. 5 as a block diagram.

4. Parameter identification

In order to use the model for the controller design and simulations, the missing parameters have to be identified and

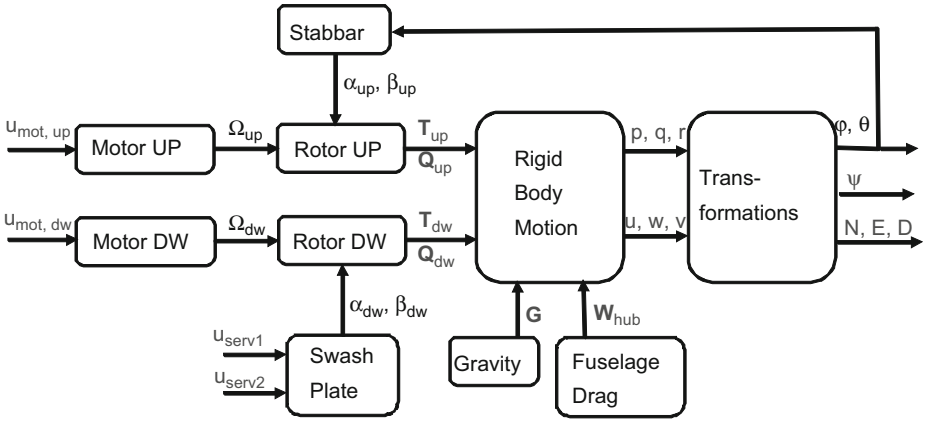

Fig. 5. muFly dynamic model block diagram.

adjusted to the real helicopter. The identification process is a non-trivial task especially since most of the parameters are coupled. In order to minimize the complexity of the identification on real flight data it is necessary to measure or estimate as many parameters as possible beforehand.

All the mechanical properties such as mass, maximal swash plate angle, gear ratio, rotor diameter or body inertias can easily be measured or determined from the CAD design. The aerodynamical coefficients c_T and c_Q, determining the thrust and torque values of the rotors, are identified by measuring the torque and thrust of the lower and upper rotor on a coaxial rotor test-bench designed for blade optimization (Schafroth, Bouabdallah, Bermes, & Siegwart, 2008). Running the test bench in coaxial configuration allows to include the thrust loss on the lower rotor due to the down wash of the upper. The parameters for the low cost off-the-shelf electro motors are not available, thus experimental data has to be used for the identification. Those motor measurements have been done by our partner CEDRAT (2009) by applying a constant voltage, varying the external torques on the motors and measuring the rotational speed and current. The motor constants are identified using the stationary solution $\dot{\omega} = 0$ of the motor equation and the least-square method (LS) (Schwarz & Kaeckler, 2004). Result plots for the identification are shown in Fig. 6.

The remaining unknown parameters are identified dynamically using real flight data. Since the equations are not static anymore, a dynamic identification process has to be used.

In this work the Covariance Matrix Adaptation Evolution Strategy (CMA-ES) (Hansen & Ostermeier, 1996) approach is used to identify the parameters of the nonlinear model. Similar to quasi-Newton methods (Nocedal & Wright, 2006), the CMA-ES is a second order approach estimating a positive definite matrix within an iterative procedure. It differs from the quasi-Newton methods in the way that instead of the inverse Hessian matrix H^{-1} the covariance matrix C is estimated. This matrix is, on convex-quadratic functions, closely related to the inverse Hessian H^{-1}. The key idea of the CMA-ES is to adapt the covariance matrix in a way that the probability to reproduce successful mutation steps is increased. Randomized search algorithms like the CMA-ES are regarded to be robust in a rugged search landscape, which can comprise discontinuities or local optima. The CMA-ES in particular is designed to tackle, additionally, ill-conditioned, non-separable, nonlinear and non-convex problems in dimensions of three to one hundred and thus it constitutes an adequate tool to identify the parameters using multiple sets of measurement data. The exact formulation of the optimization algorithm is well described in Hansen (2009). For the practical application of the CMA-ES it is important to set adequate initial conditions and, even

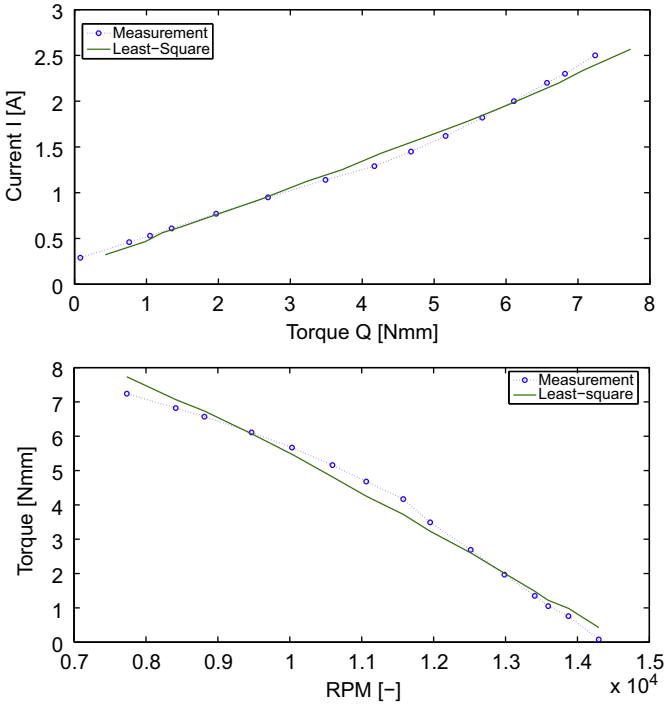

Fig. 6. Least square result plots for the electro motor parameter identification.

more important, feasible boundaries for the parameters. Otherwise the algorithm fits the simulation output to the measurement data while neglecting the physics.

For recording the flight data, the helicopter is steered by a pilot. In order to cover as much frequency bandwidth as possible, a chirp signal is generated and superimposed on the pilot input. However, the helicopter is not adequately controllable in open loop by a pilot. Therefore, an additional PID controller is used to control attitude and help the pilot. Effectively, the pilot controls the set point values of the PID controller. The controller is not problematic for the parameter identification, since the actuator signals are recorded and sent together with the sensor data. Hence the identification of the system is independent of the controller. As a visualization the identification process is shown in Fig. 7. It shows the reference value input $\mathbf{r}(t)$ of the pilot as the input of the PID controller. The output of the controller $\mathbf{u}(t)$, the motor and servo inputs, is sent to the helicopter and the nonlinear model, where a new output $\hat{\mathbf{y}}(t)$ is predicted. This output is

compared to the respective sensor measurement $\mathbf{y}(t)$ and the error ε is build and minimized by adjusting the parameters Θ using the CMA-ES.

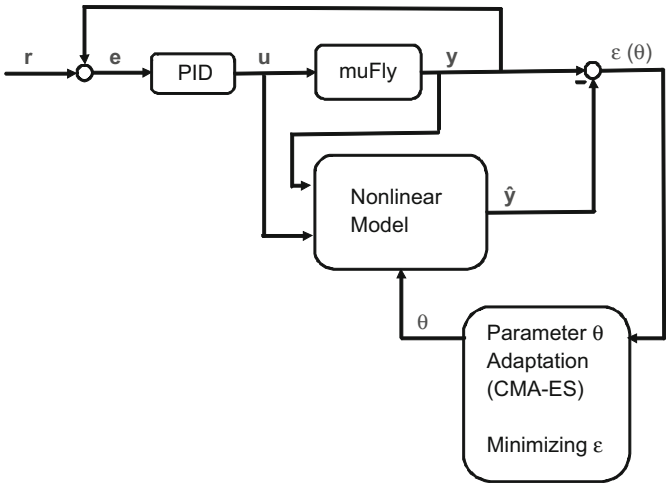

Fig. 7. The identification process block diagram.

Since only sensors for the attitude angles and the distance to the ground are mounted on the helicopter, the model is reduced by the horizontal linear motion states, resulting in a state-space system of 14 states. The identification is split into two subsystems 'heave-yaw' and 'pitch-roll'. For the heave-yaw subsystem, the parameters are identified on two datasets. In the first dataset, the altitude is kept constant and the yaw angle reference is excited, and in the second dataset vice versa. This allows a correct adjustment of the parameters since most of them act on the yaw and heave dynamics. Similar to the heave-yaw the roll and pitch are coupled due to gyroscopic effects and thus identified simultaneously. The results for the identified subsystems are shown in Figs. 8–11, respectively.

The results show a good match between the nonlinear model and the experimental data. It mainly deviates in the amplitude, which does not impose a problem in closed-loop operation, since it is covered by the gain of the controller. A table with all the identified parameters is shown in Table 1 in the appendix.

5. Controller design

The control structure for full position control of muFly is shown in Fig. 12. It consists of three multi-input multi-output (MIMO) controllers: the first controls the heave z and the yaw

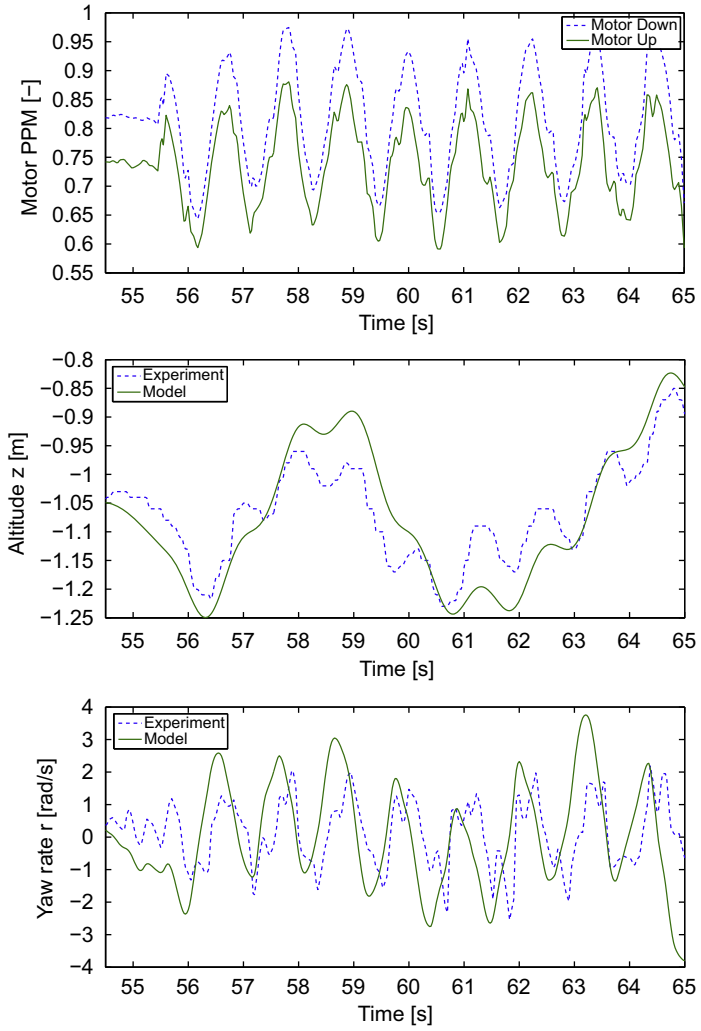

Fig. 8. CMA-ES identification result plots for an actuation in heave. UP: Motor input signals. MID: Ultra sonic altitude measurement and model. DW: IMU yaw rate measurement and model.

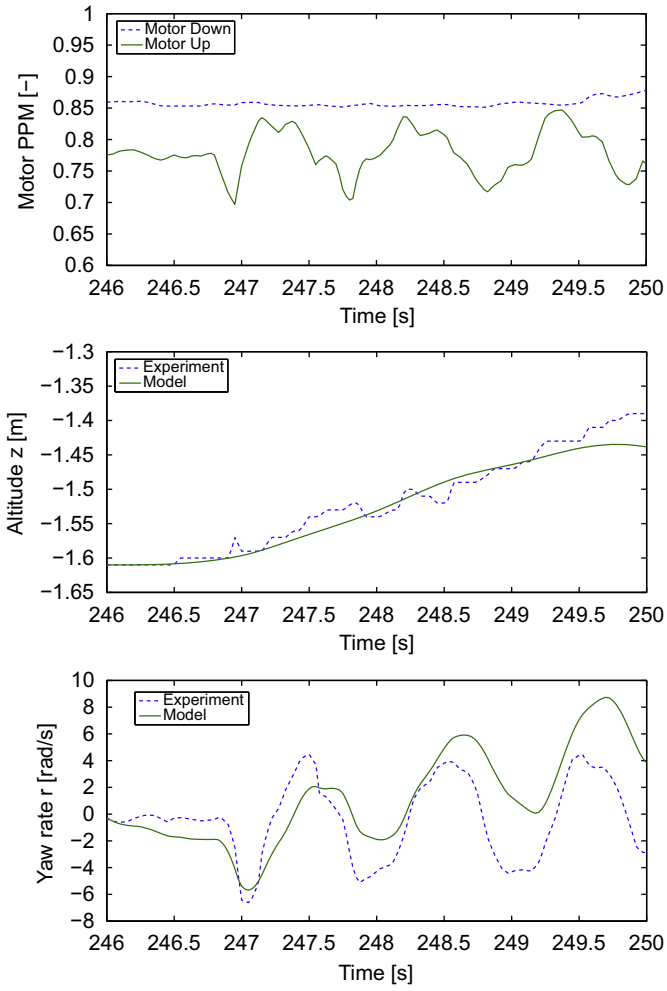

Fig. 9. CMA-ES identification result plots for an actuation in yaw. UP: Motor input signals. MID: Ultra sonic altitude measurement and model. DW: IMU yaw rate measurement and model.

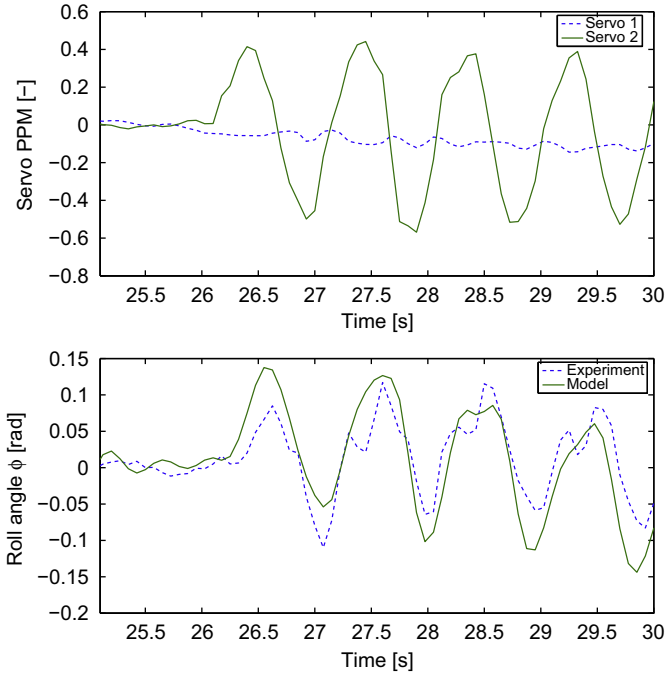

Fig. 10. CMA-ES identification result plots for an actuation in roll. UP: Servo input signals. DW: IMU roll angle measurement and model.

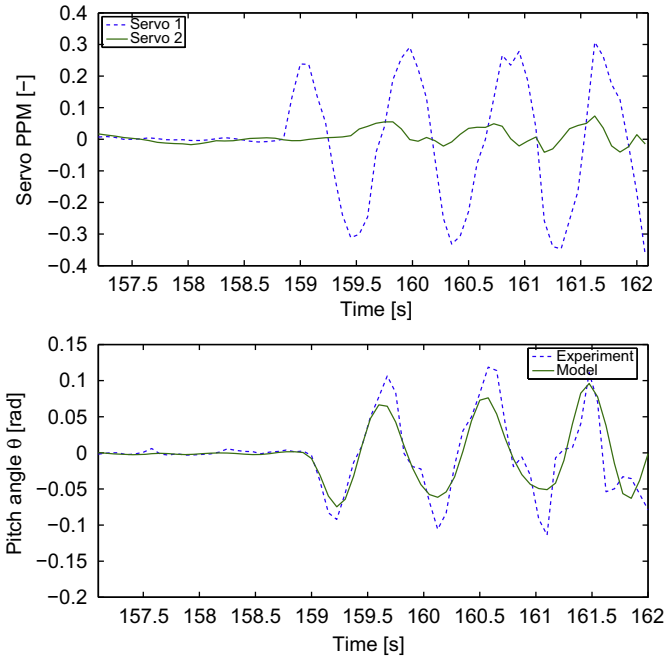

Fig. 11. CMA-ES identification result plots for an actuation in pitch. UP: Servo input signals. DW: IMU pitch angle measurement and model.

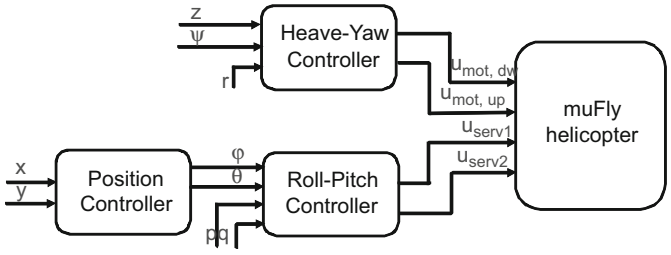

Fig. 12. Control structure for muFly.

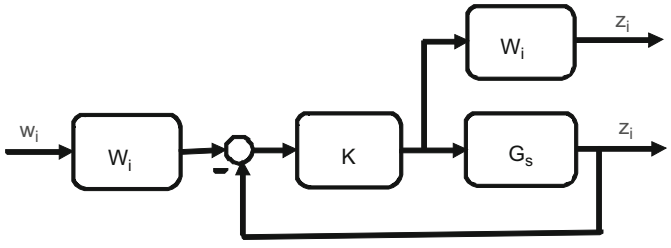

Fig. 13. Illustration of the weighting for the H_∞- control design.

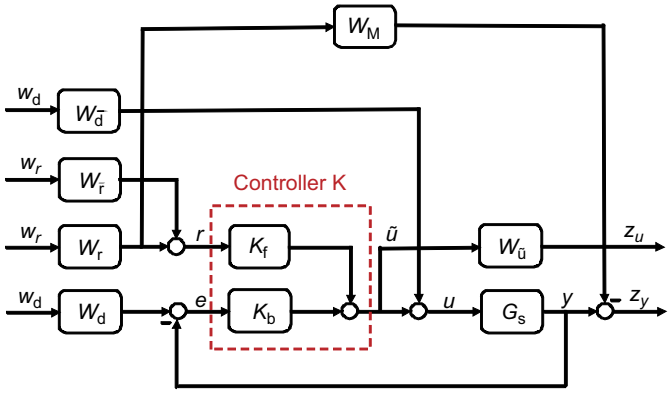

Fig. 14. The dual 2-dof *GS*/*T*-weighting scheme.

angle ψ via the two rotor speeds, the second controls the roll ϕ and pitch θ angles using the swash plate inputs (servos), and the last sets the reference inputs ϕ and θ for the roll-pitch controller for a tight position reference tracking. As mentioned in Section 3 the sensor hardware for the position measurement is not ready yet, so the focus in this paper is on the heave-yaw and roll-pitch controller.

The designated missions for muFly do not require fast maneuvers of the helicopter. Slow maneuvers and tight control around the hover point are more important. Hence it seems a reasonable choice to use linear control techniques for the controller design. In this work a mixed sensitivity H_∞ optimization is used for the two controllers. The theory of H_∞ controllers can be found in various sources (e.g. Skogestad & Postlethwaite, 2005), thus only an outline and the specific parts of the controllers used in this work are given.

For the H_∞- control design, the plant G_s to be controlled is augmented by the dynamical weights W_i described in the frequency domain. Using those weights allows to shape the (in general closed loop) behavior of the control system by minimizing

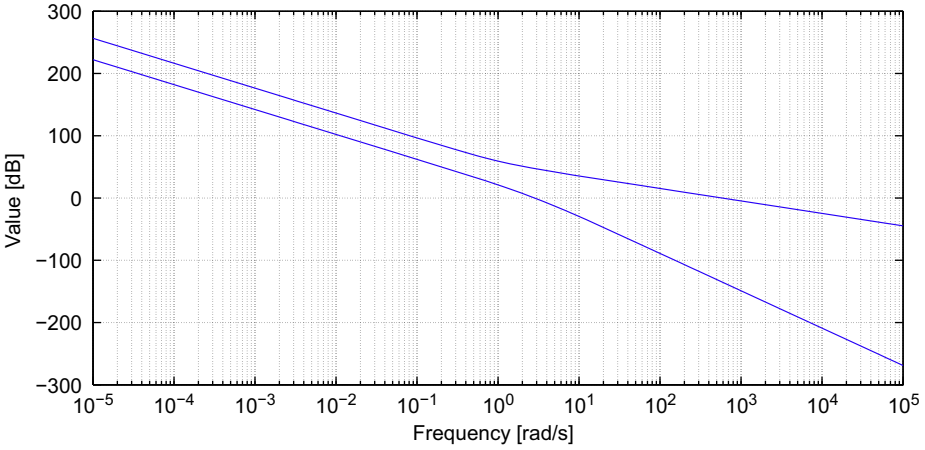

Fig. 15. Singular value plot of the heave-yaw subsystem.

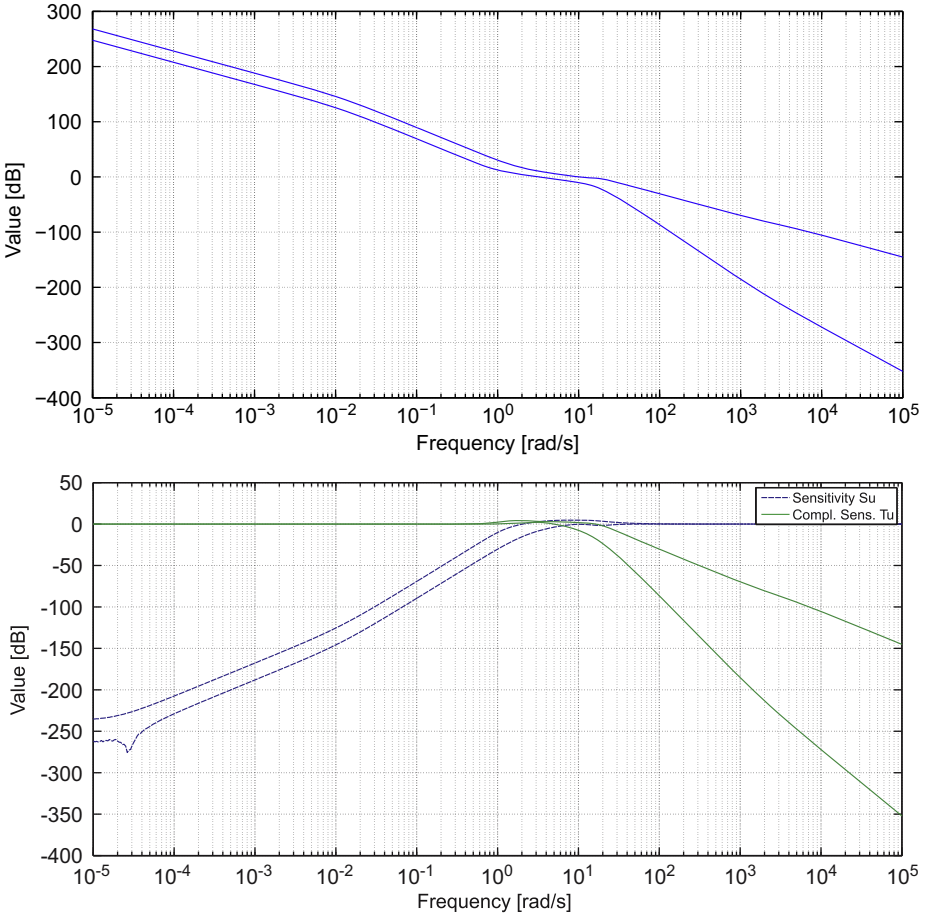

Fig. 16. Singular value plots of the heave-yaw plant loop gain L_u (UP), the sensitivity S_u and the complementary sensitivity $T_u$transfer function (DW).

the H_∞- norm of the transfer function T_{zw} resulting in the controller K. An illustration of the weighting principle is displayed in Fig. 13.

Both controllers are designed using the dual $(y>u)$ GS/T-weighting scheme (Geering, 2004), where the product of the plant G_s with the sensitivity S and the complementary sensitivity T are shaped by the weights W_i. However, the controllers differ in their structure. While for the roll-pitch control a pure feedback controller is used, a two degree of freedom (2-dof) approach (Horowitz, 1963) is taken for the heave-yaw control. This means the controller K consists of two sub-controllers, a controller K_f for feedforward reference input and a controller K_b for feedback control as shown in Fig. 14. The reason for the choice of a feedforward part is the desired tight reference following for altitude and heading. The feedforward part minimizes overshoots in the altitude, which is a critical aspect in the foreseen missions. On the downside it needs more processing power, which is limited on the micro-controller. The main task of the pitch-roll controller is to stabilize the system, and only small reference changes will be given by the position controller, so a pure feedback controller should be adequate.

For the application of the H_∞- technique the nonlinear model from Section 3 has to be linearized around the operation point, in this case hover. Similar to Section 4 the model is split in two subsystem and linearized resulting in two state-space system of 6 states for heave-yaw and 8 states for roll-pitch.

5.1. Heave-yaw control

The dual 2-dof GS/T-weighting scheme of the heave-yaw controller is shown in Fig. 14 and has the corresponding transfer function T_{zw}

$$T_{zw}=\begin{bmatrix} -W_{\ddot{u}}T_uW_{\bar{d}} & G_sS_uW_{\bar{d}} \\ W_{\ddot{u}}S_uK_fW_{\bar{r}} & T_{yr}W_{\bar{r}} \\ W_{\ddot{u}}S_uK_fW_r & (T_{yr}-W_M)W_r \\ W_{\ddot{u}}S_uK_bW_d & T_eW_d \end{bmatrix}^T.$$

If the H_∞- problem has a solution $\|T_{zw}\|_\infty \le \gamma$ with $\gamma \le 1$, the specifications for the sensitivities are fulfilled. However, technically it is not necessary to achieve the value $\gamma=1$, a small value for γ is sufficient for an asymptotically stable and robust system (Geering, 2004).

In Fig. 15the singular values of the linearized heave-yaw plant G_s is shown. The cross over frequency is at 2.82 rad/s and the plant shows an integrating character. This means that theoretically an integrating part of the controller is not needed, but nevertheless the controller is designed to have poles close to the imaginary axis, thus having integrating character. This compensates for the battery voltage drop during operation, requiring a higher motor input signal with time.

The controllers K_f and K_b are then designed using following weights augmented to their right dimensions

$$W_{\ddot{u}}(s)=0.001,\quad W_d(s)=\frac{s+10}{0.1s+20},$$

$$W_{\bar{d}}(s)=\frac{0.7s+1}{s+0.7/100},\quad W_{\bar{r}}(s)=\frac{s+7}{0.01s+14},$$

$$W_r(s)=\frac{s^2+15s+14}{10^{-4}s^2+14s+0.0014},\quad W_M(s)=\frac{14}{s+14}.$$

The meaning of the weights is as follows: the weight $W_{\ddot{u}}(s)$ is used to minimize the influence of the second row (can be neglected). The weight $W_{\bar{d}}^{-1}(s)$ is a boundary for the complementary sensitivity $T_e(s)$, $W_{\bar{r}}^{-1}(s)$ for the complementary sensitivity $T_{yr}(s)$ and $W_{\bar{d}}(s)$ is used to shape the sensitivity $S_u(s)$. The two weights $W_M(s)$ and $W_r(s)$ are used as a reference model for $T_{yr}(s)$ and as an upper boundary for the model-matching error, respectively.

Solving the H_∞ problem results in a $\gamma=1.38$. The resulting transfer functions for the loop-gain L_u, sensibility S_u and complementary sensibility T_u are shown in Fig. 16. The cross-over frequency is at $\omega_c=3.26$ rad/s while as the maximum sensitivity and the maximum complementary sensitivity peak are at $S_{u,\max}$ = 3.7398 dB and $T_{u,\max}$ = 3.93 dB.

The result of the closed-loop simulation to a step input in heave (-0.5 m, negative means upwards) on the nonlinear plant is plotted in Fig. 17. In this condition the helicopter can easily follow the reference step in heave without overshoots (the same result was found for a step response in yaw).

Measurements of a corresponding flight experiment on the real system are plotted in Fig. 18. As expected, the real system shows a slightly worse performance due to small model deviations and noisy data. Especially the control in yaw direction is not as tight as predicted by simulation. A reason might be the strong drift of the yaw measurement from the IMU. The heave control shows a good correlation with the prediction of the simulation, having only a small overshoot, but considering the scale the deviation is very small. Overall the performance for the heave-yaw control is satisfying.

Furthermore, the robustness of the H_∞ controller is tested in simulation by varying threes system parameters from their

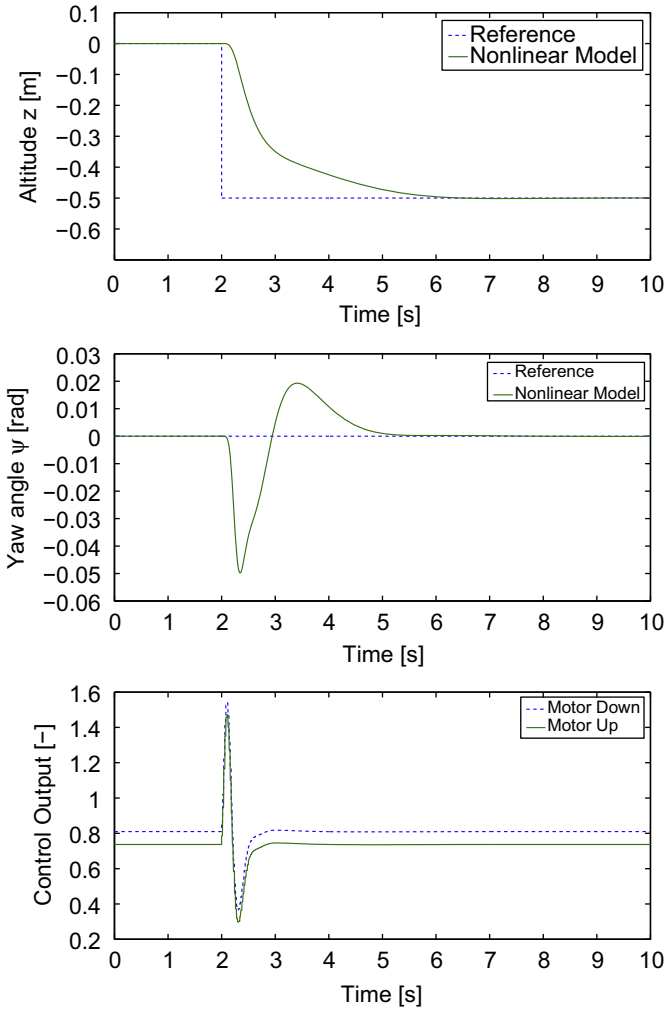

Fig. 17. Simulation result plots for a closed-loop step response in heave.

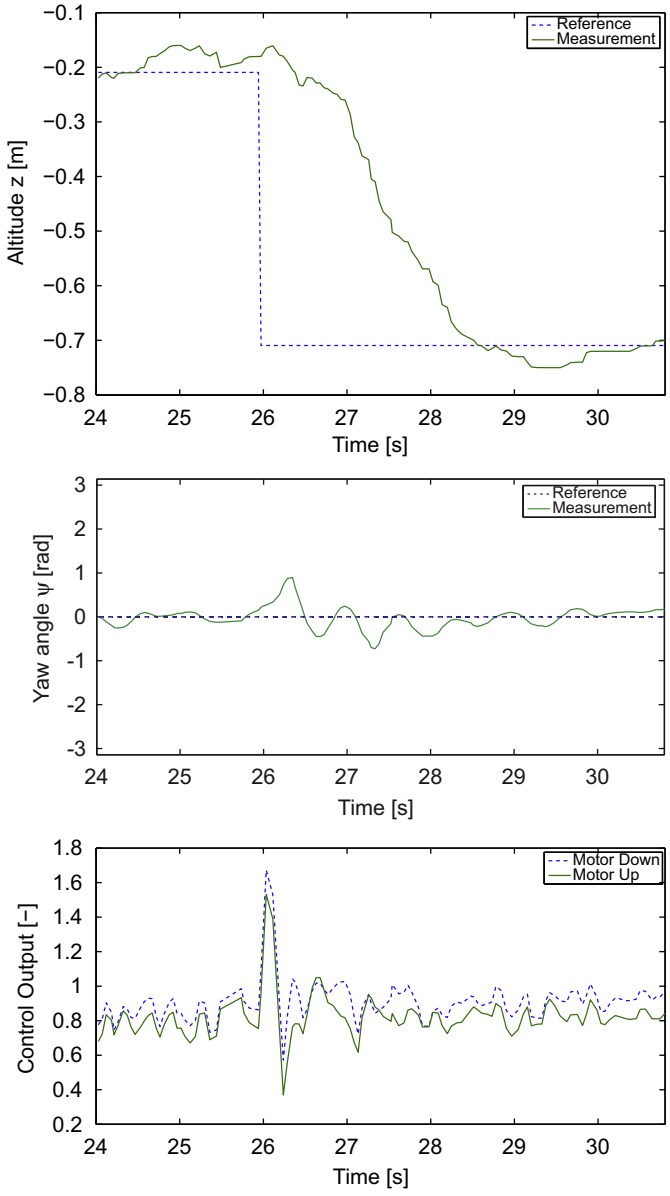

Fig. 18. Measurement result plots for a step response in heave.

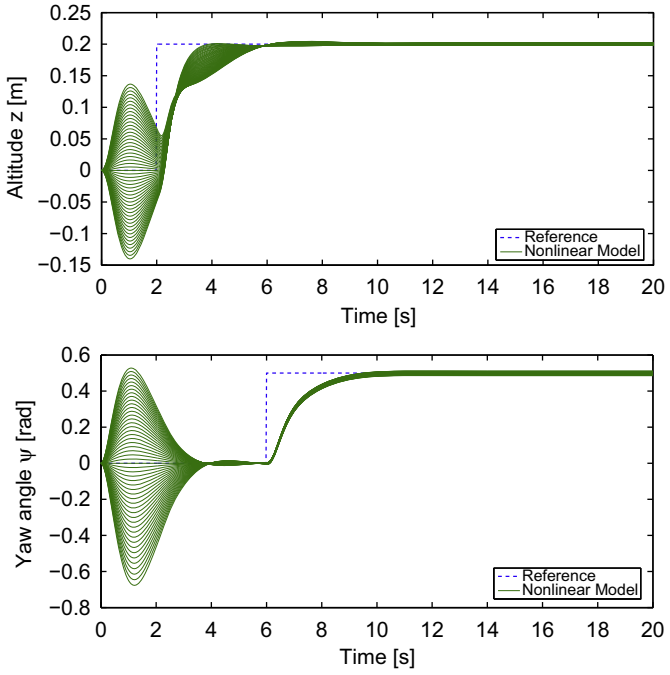

Fig. 19. Robustness simulation for a step input in heave (2 s) and yaw (6 s).

nominal value, the upper thrust and torque coefficients $c_{T\,\mathrm{up}}$, $c_{Q\,\mathrm{up}}$ and the upper drive train inertia $J_{\mathrm{drive,up}}$. This corresponds to a deviation of the identified system parameters from the real values. In Fig. 19, the results for a step input in heave and yaw for a deviation range of $\pm 20\%$ for the three parameter is plotted. It shows that the controller can handle strong deviations in the system parameters. It mainly suffers in the beginning due to the implied difference in the operation points. As soon as the difference is compensated, the performance is similar to the simulation with correct parameters. Additionally, a small steady state error is seen, due to the chosen weights, which place the poles only close to the imaginary axis and not on the imaginary axis itself (no pure integrator).

5.2. Roll-pitch control

The procedure for the roll-pitch control is similar to the heave-yaw control, it differs only in the weighting scheme due to the missing feedforward controller K_f. Thus, it is abandoned to show it here and present only the key elements.

The singular value plot of the linearized roll-pitch plant is shown in Fig. 20. The bandwidth of the system is very low, which is caused by the stabilizer bar. Additionally the resonance frequency peak at 14.5 rad/s leads to problems in the closed-loop design, as it can be seen in Fig. 20, where the influence of the peaks on the loop-gain L_u, sensibility S_u and complementary sensibility T_u is clearly visible. It is desirable to have those peaks after the cut off frequency, therefore the controller is designed to have a low bandwidth of 2 rad/s. Since the main task of the roll-pitch control is to support the insufficient stabilization of the stabilizer bar and follow moderate reference angles from the position controller, this should be adequate. Another solution to reduce the effect of the resonance peak might also be to modify the weights W_i (Fig. 21).

In Fig. 22 the simulation results for a reference tracking in pitch is shown as a comparison to the measured data in Fig. 23, where the reference values are set by the pilot's remote control. In this measurement the real system is able to follow the reference slightly better than the model prediction. Here a reason might be that the nonlinear model underestimates the dynamics of the system in pitch. Nevertheless, the influence of the stabilizer bar on the dynamics is strong and it might be considered to remove it from the helicopter in future for better control authority.

6. Conclusions

In this paper the design procedure for a robust control of the coaxial micro helicopter muFly using H_∞- controller techniques is presented. As a first step, a nonlinear model is developed. An appropriate model is essential for the controller design and simulations. The model is based on the rigid body dynamics, where all the possible acting forces and moments are discussed. Further, the dynamics of the mechanical devices such as the

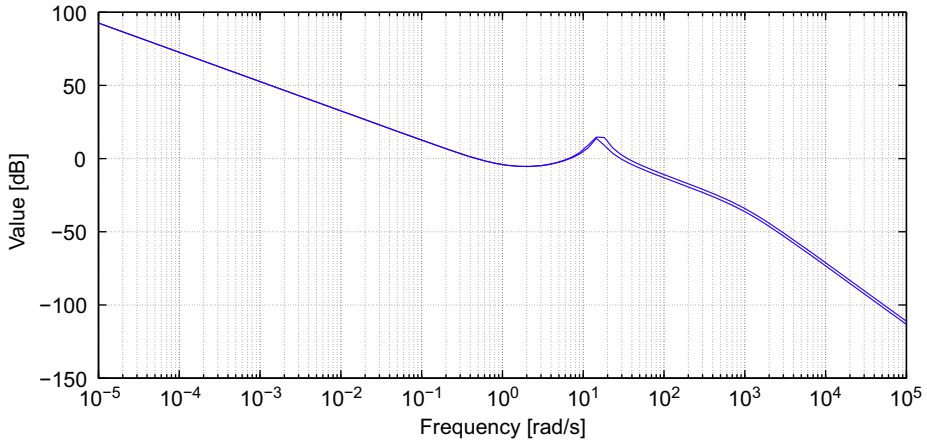

Fig. 20. Singular value plot of the roll-pitch subsystem with stabilizer bar.

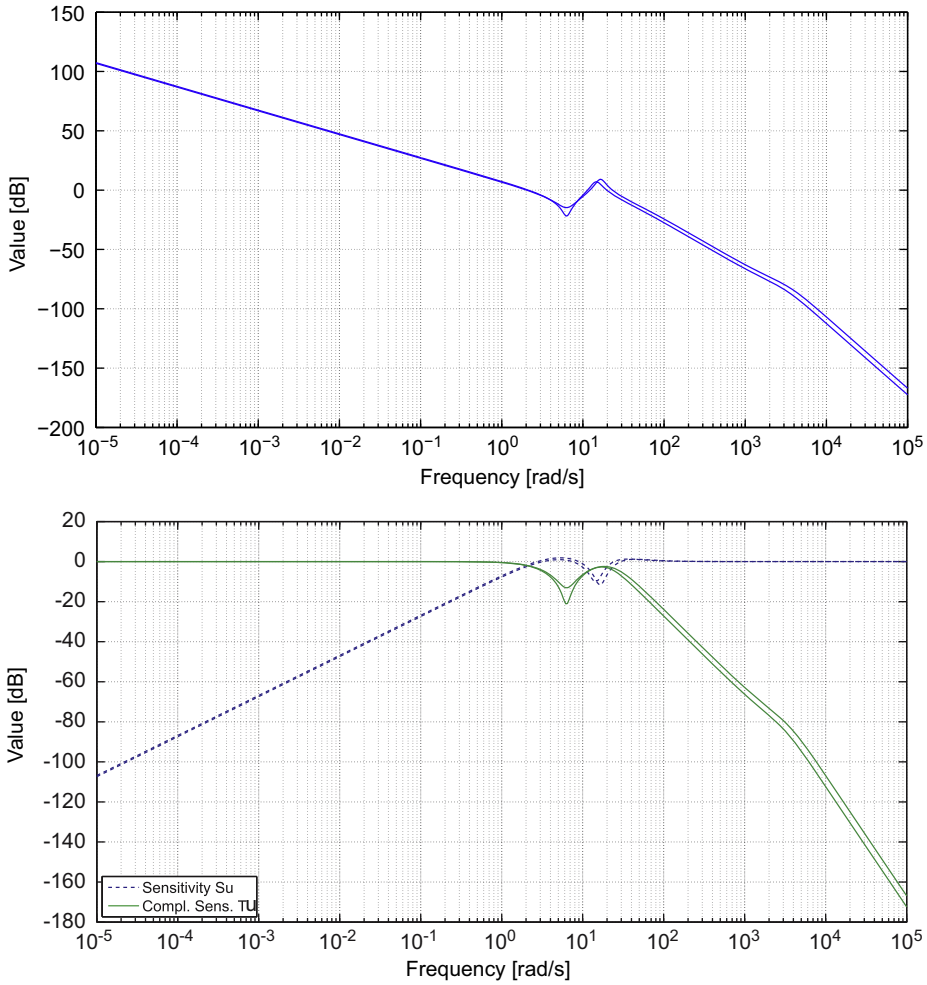

Fig. 21. Singular value plot of the roll-pitch subsystem loop gain L_u (UP), sensitivity S_u and the complementary sensitivity T_u transfer functions (DW).

swash plate, electro motor and stabilizer bar are derived, resulting in a complete structured model. However, a good model with incorrect parameters is worthless, hence those parameters have to be identified. While most parameters are measured using CAD data or test benches, some parameters have to be identified from real flight data applying identification methods. For this task a randomized search algorithm, the Covariance Matrix Adaptation Evolution Strategy (CMA-ES), is used. This allows to identify

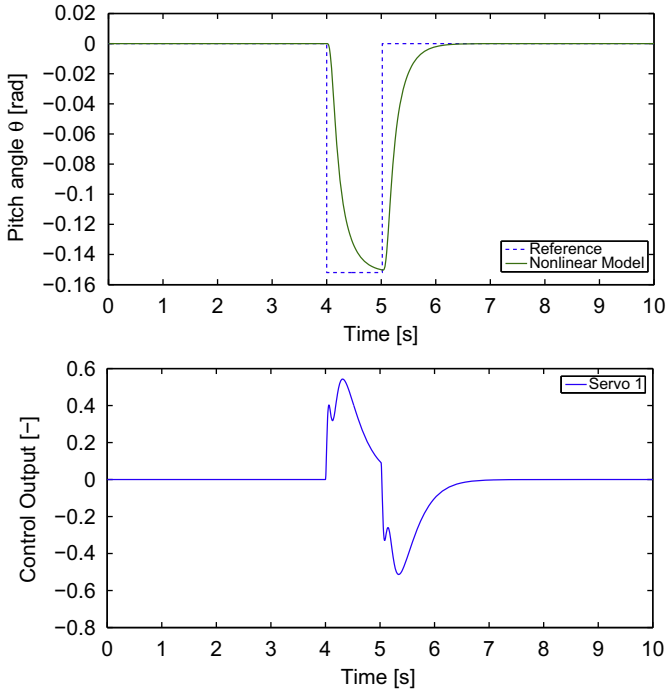

Fig. 22. Simulation result plot for a reference following in pitch.

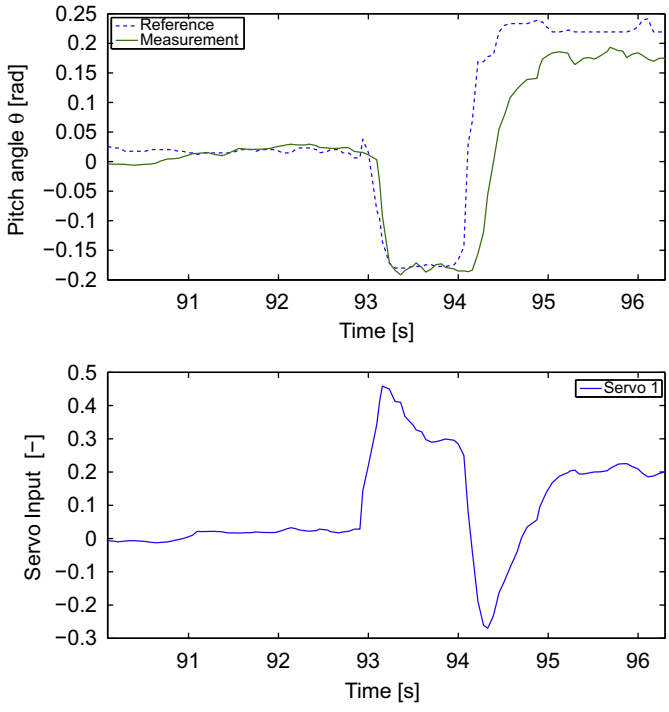

Fig. 23. Measurement result plots for a reference following in pitch. The reference is applied by the pilot with the RC stick.

multiple parameter on multi-dimensional data. The parameters are successively identified showing the appropriateness of the nonlinear model.

The identified model is then used for the design of the controllers for the heave-yaw and roll-pitch subsystems. The controllers are designed applying a mixed sensitivity H_∞-optimization using the *GS*/*T*-weighting scheme.

In conclusion it can be said that the controllers are successfully tested on the real system showing the appropriateness of the overall design procedure. It showed that this design procedure fits well for this application, but it can also be used for other more general applications. On the other hand there is still some margin to improve the implemented controllers in near future.

As another future work the performance might be improved using nonlinear control techniques such as feedback linearization or gain scheduling. In addition there is the idea to remove the stabilizer bar from the helicopter and stabilize it actively. Beside a better control authority this would increase the autonomy time due to reduced drag force. The last task is to design the position control as soon as the sensor for position measurement is available.

Acknowledgments

The authors would like to thank Mr. S. Leutenegger, Mr. T. Baumgartner, Mr. F. Haenni, Mr. M. Buehler and Mr. D. Fenner. muFly is a STREP Project under the Sixth Framework Programme of the European Commission, Contract no. FP6-2005-IST-5-call 2.5.2 Micro/Nano Based Sub-Systems FP6-IST-034120. The authors gratefully acknowledge the contribution of our muFly Project partners BeCAP at Berlin University of Technology, CEDRAT Technologies, CSEM, Department of Computer Science at University of Freiburg and XSENS Motion Technologies.

Appendix A

A table with all the identified parameters is shown in Table 1.

Table 1
Identified parameters.

Parameter	Description	Value	Unit
m	Mass	0.095	kg
I_{xx}	Inertia around x-axis	$1.12e^{-4}$	kg m^2
I_{yy}	Inertia around y-axis	$1.43e^{-4}$	kg m^2
I_{zz}	Inertia around z-axis	$2.66e^{-5}$	kg m^2
z_{dw}	Distance CoG lower rotor hub	−0.051	m
z_{up}	Distance CoG upper rotor hub	−0.091	m
$\Theta_{\mathrm{SP,max}}$	Maximal swash plate angle	15	deg
R	Rotor radius	0.0875	m
$c_{T\ \mathrm{dw}}$	Thrust coefficient lower rotor	0.0117	–
$c_{T\ \mathrm{up}}$	Thrust coefficient upper rotor	0.0138	–
$c_{Q\ \mathrm{dw}}$	Torque coefficient lower rotor	0.0018	–
$c_{Q\ \mathrm{up}}$	Torque coefficient upper rotor	0.0025	–
$J_{\mathrm{drive,dw}}$	Drive train inertia (down)	$7.04e^{-6}$	kg m^2
$J_{\mathrm{drive,up}}$	Drive train inertia (up)	$2.11e^{-5}$	kg m^2
κ_{E}	Electrical motor constant	0.0045	V^{-1} s^{-1}
κ_{M}	Mechanical motor constant	0.0035	Nm A^{-1}
d_{R}	Motor friction	$5.2107e^{-7}$	Nm s
R_Ω	Resistance	1.3811	Ω
i_{gear}	Gear ratio	1.5	–
η_{gear}	Gear efficiency	0.84	–
W_{hub}	Drag force on the fuselage	0.009	N
$T_{\mathrm{f,dw}}$	Following time upper rotor	0.001	s
$T_{\mathrm{f,up}}$	Following time upper rotor	0.24	s
l_{dw}	Linkage factor upper rotor	0.77	–
l_{up}	Linkage factor lower rotor	0.48	–

References

Bermes, C., Leutenegger, S., Bouabdallah, S., Schafroth, D., & Siegwart, R. (2008). New design of the steering mechanism for a mini coaxial helicopter. In *IEEE international conference on intelligent robots and systems (IROS)*, Nice, France.

Bohorquez, F., Rankinsy, F., Baederz, J., & Pines, D. (2003). Hover performance of rotor blades at low Reynolds numbers for rotary wing micro air vehicles. An experimental and CFD study. AIAA Applied Aerodynamics Conference, Orlando, USA.

Bouabdallah, S., & Siegwart, R. (2005). Backstepping and sliding-mode techniques applied to an indoor micro quadrotor. In *Proceedings of the 2005 IEEE international conference on Robotics and automation* (*ICRA 2005*) (pp. 2247–2252).

Bramwell, A. (2001). *Helicopter dynamics (2nd ed.)*. London: Butterworth, Heinemann.

CEDRAT (2009). CEDRAT Technologies 〈http://www.cedrat.com〉 (01/28/2009).

Epson (2004) 〈http://www.epson.co.jp/e/newsroom/news_2004_08_18.htm〉 (01/28/2009).

Geering, H. P. (2004). *Robuste regelung*. Technical report, ETH Zurich.

Hansen, N. (2009). *The CMA evolution strategy*: *A tutorial*. Technical report.

Hansen, N., & Ostermeier, A. (1996). Adapting arbitrary normal mutation distributions in evolution strategies: The covariance matrix adaptation. In *IEEE international conference on evolutionary computation*, Nagoya University, Japan.

Horowitz, I. M. (1963). *Synthesis of feedback systems*. New York: Academic Press.

Leishman, J. (2006). *Helicopter aerodynamics* (2nd ed). Cambridge.

Leitner, J., Calise, A., & Prasad, J. V. R. (1997). Analysis of adaptive neural networks for helicopter flight controls. *Journal of Guidance*, *Control*, *and Dynamics*, *20*(5), 972–979.

Mettler, B. (2003). *Identification modeling and characteristics of miniature rotorcraft*. Dordrecht: Kluwer Academic Publishers.

Mettler, B., Kanade, T., & Tischler, M. (2000). *System identification modeling of a model-scale helicopter*. Technical report, Robotics Institute, Carnegie Mellon University.

Mueller, G., & Ponick, B. (2006). *Elektrische maschinen grundlagen elektrischer maschinen*. Weinheim: VCH.

Nocedal, J., & Wright, S. (2006). *Numerical optimization*. Berlin: Springer.

Schafroth, D., Bermes, C., Bouabdallah, S., & Siegwart, R. (2009). Modeling and system identification of the mufly micro helicopter. In *Second international symposium on unmanned aerial vehicles UAV'09*, Reno, USA.

Schafroth, D., Bouabdallah, S., Bermes, C., & Siegwart, R. (2008). From the test benches to the first prototype of the muFly micro helicopter. *Journal of Intelligent and Robotic Systems*, *54*(1–3), 245–260.

Schwarz, H. R., & Kaeckler, N. (2004). *Numerische mathematik*. Stuttgart, Leipzig, Wiesbaden: Teubner.

Skogestad, S., & Postlethwaite, I. (2005). *Multivariable feedback control: Analysis and design*. New York: Wiley. (1121635).

Wade, R. L., & Walker, G. W. (1996). Flight test results of the fuzzy logic adaptive controller-helicopter (FLAC-H). In *Society of photo-optical instrumentation engineers* (*SPIE*) *conference series*.

Walker, D. J. (2003). Multivariable control of the longitudinal and lateral dynamics of a fly-by-wire helicopter. *Control Engineering Practice*, *11*(7), 781–795 , doi:10.1016/S0967-0661(02)00189-2.

Wang, W., Song, G., Nonami, K., Hirata, M., & Miyazawa, O. (2006). Autonomous control for micro-flying robot and small wireless helicopter X.R.B. In *IEEE international conference on intelligent robots and systems*, Beijing, China.

Zhao, L., & Murthy, V.R. (2009). Optimal controller for an autonomous helicopter in hovering and forward flight.